Effects of Bimodal Beam Shaping on Melting And Resolidification of Stainless Steel

Marco Rupp^{1,2}, Shuichiro Hayashi^{1,2}, Ankit Das^{1,2}, Michael Schmidt^{3,4}, and Craig B. Arnold*^{1,2}

¹Department of Mechanical and Aerospace Engineering, Princeton University, 08544, NJ, USA

²Princeton Materials Institute, Princeton University, Princeton, 08544, NJ, USA

³Erlangen Institute of Photonic Technologies (LPT), Friedrich-Alexander-Universität ErlangenNürnberg, 91052 Erlangen, Germany

⁴Erlangen Graduate School in Advanced Optical Technologies (SAOT), 91052 Erlangen, Germany *Corresponding author's e-mail: cbarnold@princeton.edu

Laser processing offers precise control over conventional techniques, but the lack of control over microstructure. Traditional single-mode beam strategies often result in steep thermal gradients and columnar grain growth. In this study, we introduce a bimodal beam scanning approach in which one laser beam scans steadily while a second laser beam oscillates perpendicularly to the scan direction at a controlled frequency and amplitude. By modulating the spatial distribution of the energy input during scanning, this technique enables dynamic shaping of the melt pool geometry. Cross-sectional analysis reveals that while unmodulated tracks exhibit elongated columnar grains, modulated tracks display more equiaxed grains. Differences observed in both melt pool geometry and microstructure between the steady single-mode and the bimodal laser scan prompted three-dimensional thermal simulations to investigate the underlying thermal mechanisms. These simulations were used to examine how beam modulation affects temperature profiles and gradients, helping to explain the resulting variations microstructure. This dynamic beam shaping approach offers a promising pathway for laser-based metal processing, to achieve a more equiaxed microstructure.

DOI: 10.2961/ilmn.2025.03.2018

Keywords: dynamic beam shaping, microstructure, laser processing, advanced manufacturing, laser-material interaction

1. Introduction

Laser technology plays an important role in modern manufacturing, with applications ranging from process monitoring[1], quality control, to material processing[2]. Laser processing's ability to not only interact with a wide range of materials, including ceramics[3], polymers[4–6], and metals[2,7], but also deliver high precision and digital customizability, makes it suitable for the fabrication[8] and modification[9] of complex parts. However, during high-power laser processes, such as metal additive manufacturing[10] and welding[11], the rapid heating and cooling of the metallic material can introduce a range of defects[12]. Defects may appear on a surface level as features in the form of humps[13] and balls[14] or occur beneath the surface in the form of pores[15] and cracks[16].

Beyond these defects, elongated microstructures, or columnar grains, can result in undesirable mechanical anisotropy[17] and limit component performance. The formation of elongated, columnar grains in conventional laser processing is closely tied to the steep thermal gradients induced by Gaussian beam profiles, which promote directional solidification along the heat flow [18]. To mitigate columnar grain formation, beam shaping strategies, such as beam wobbling[19], intensity modulation[20], and multi-laser configurations[21,22], have emerged as promising techniques. These methods aim to reduce thermal gradients, and enhance the formation of small aspect ratio microstructures, or equiaxed grains[18], which are

associated with improved isotropy and resistance to defect propagation[23].

Among beam shaping approaches, bimodal-laser configurations, which superimpose two independent lasers at spatial offsets, provides spatiotemporal versatility and adaptive control over spatial energy distribution. Previous studies on bimodal-laser processing demonstrated improvements in surface quality and the ability to locally modulate heat input without altering total energy[24], making it a promising method for advanced manufacturing systems. However, prior work focused on macroscopic geometrical effects and the underlying microstructural effects remain unclear.

In this study, the impact of a bimodal-laser processing comprising of one steady and one oscillating beam, on metal microstructures is investigated. Through a combination of experimental characterization and transient thermal simulations, the effects of temperature gradient reductions on microstructure are examined and compared to a conventional single-mode processing case. This approach offers a pathway to enhance and ultimately control the microstructure in metal-based laser processes.

2. Experimental

For all experiments conducted in this study, stainless steel metal plates (SS316L) with a thickness of 1.5 mm were used as the target metal material.

2.1 Intensity distribution modulation

To study the effects of sinusoidal intensity distribution modulation on microstructure in laser-based metal processing, two continuous-wave (CW) laser systems from IPG Photonics, USA, were used simultaneously. Both laser systems, a YLR-100 with a maximum output of 100 W and a YLR-400 with a maximum output of 400 W, are independently tunable and generate laser beams with a central wavelength of 1060 nm. For all experiments, the total laser power was set to 200 W. In the single-mode case only one laser system was used with a power of 200 W, while in the bimodal case each laser system was set to 100 W. The simultaneous scanning of the laser beams across the metal surfaces was achieved by using two independent Focus Shifter digital galvanometer laser scanner systems (Raylase GmbH, Germany) and focusing the beams at the same location (Fig. 1). The spot size of each laser beam at the surface was ~100 µm. The scan speed along the scan direction was kept constant for all experiments at 100 mm/s.

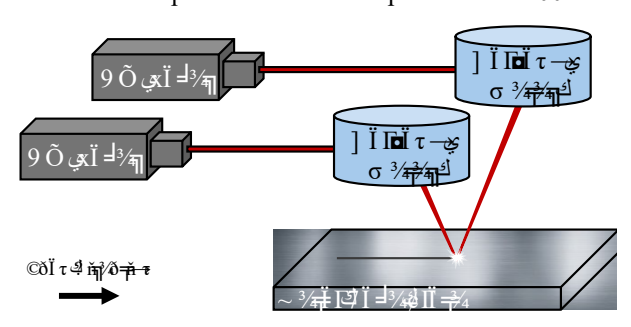


Fig. 1 Schematic of the laser setup consisting of two CW-lasers and two galvanometers focusing the respective beams onto a metal base plate.

2.2 Characterization of melt tracks

To prepare samples for cross-sectional analysis, the metal plate was cut perpendicular to the direction of the melt track using a diamond saw with cooling fluid. The resulting metal pieces were mounted using a hot-press mounting system (SimpliMet 4000, Buehler, Switzerland) for polishing. Polishing was carried out in successive steps using emery papers of increasing fineness, culminating with a 4000-grit finish to produce a reflective, mirror-like surface. After polishing, the samples were etched for 20 seconds in a chemical solution consisting of 10 mL acetic acid (17.4 M), 15 mL hydrochloric acid (12 M), 10 mL nitric acid (15.7 M), and a drop of glycerol (purity ≥99.5%). Etched samples were rinsed with distilled water and thoroughly dried. Detailed characterization of the melt pool cross-sections and surface morphologies was performed using a scanning electron microscope (SEM, Quanta 200 FEG, Thermo Fisher Scientific, USA).

2.3 Modeling of melt tracks

A three-dimensional thermal simulation was performed using COMSOL Multiphysics® to model the temperature distribution during laser irradiation. The overall simulation workflow, meshing, and a sample image are illustrated in Fig. 2. The simulation focuses exclusively on heat transfer phenomena and does not incorporate fluid dynamics or phase transformations. Key thermophysical, material, and geometric parameters were defined globally within the COMSOL environment. A custom material entry was created to incorporate the temperature-dependent properties

of stainless steel 316L, based on data reported by Kim and Mills[25,26]. The simulation employed the "Heat Transfer in Solids" physics module, with appropriate boundary conditions applied to account for convective heat loss along selected edges and radiative heat exchange with the ambient environment. In this study, two Gaussian laser beams with identical spot sizes were implemented.

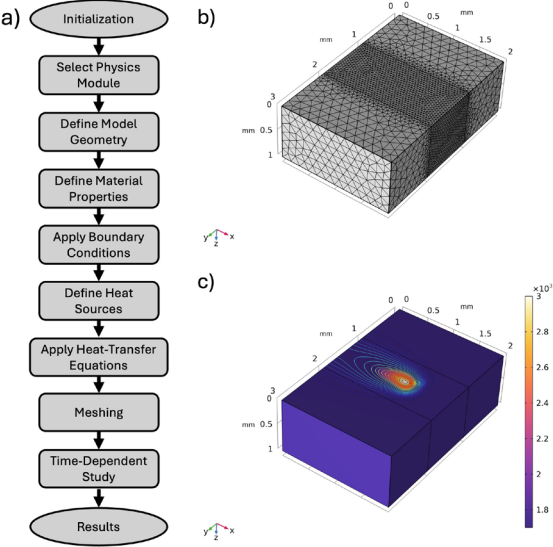


Fig. 2 (a) Schematic of COMSOL® Multiphysics Simulation workflow. (b) mesh. (c) sample picture of

The laser heat input Q(x, y, z, t) was defined using a modified Gaussian distribution,

$$Q(x, y, z, t) = Q_0 (1 - R_c) \frac{A_c}{\pi \sigma_x \sigma_y} GD A_D, \qquad (1)$$

where Q_0 represents the total laser power, R_c is the reflection coefficient, and A_C is the absorption coefficient. The terms σ_x and σ_y denote the beam radii along the x- and y-directions, respectively. GD represents the gaussian distribution in the xy-plane

$$GD = e^{-\left[\frac{(x-x_0(t))^2}{2\sigma_X^2} + \frac{(y-y_0(t))^2}{2\sigma_Y^2}\right]},\tag{2}$$

where the beam center coordinates, $x_0(t)$ and $y_0(t)$ represent the time-dependent position of the beam center and vary with time and follow either a linear or sinusoidal path depending on the laser motion. A_D represents the energy attenuation in the z-direction due to material absorption

$$A_D = e^{-A_C z}. (3)$$

For the steady single-mode (non-oscillating) laser, the beam path is linear:

$$x_0(t) = x_{00} + vt. (4)$$

$$y_0(t) = 0. (5)$$

For the oscillating laser, the path includes a sinusoidal component:

$$x_0(t) = x_{00} + vt. (6)$$

$$y_0(t) = A\sin(2\pi f t). \tag{7}$$

Heat transfer within the solid domain was governed by Fourier's law:

$$\dot{q} = -k \,\nabla T,\tag{8}$$

where \dot{q} is defined as the heat flux density and k represents the thermal conductivity. Convective and radiative boundary conditions were applied to model surface cooling, respectively:

$$\dot{q} = h \nabla T. \tag{9}$$

$$\dot{q} = h\nabla T. \tag{9}$$

$$\dot{q} = \sigma e A (T^4 - T_0^4). \tag{10}$$

The computational domain was discretized into a mesh comprising 310,701 domain elements, 12,018 boundary elements, and 456 edge elements. The simulation captured both spatial and temporal temperature variations, enabling detailed thermal profiling of the laser interaction with the material. The three-dimensional model allowed for direct comparison between simulated temperature distributions and experimentally obtained melt pool geometries from cross-sectional analysis.

3. Results and Discussion

One CW laser beam was scanned steadily across the surface of a 316L stainless steel substrate (Fig. 3a) with a Gaussian intensity distribution typical of a single-mode profile (Fig. 3b). Fig. 1c shows an SEM image of a melt track formed by single-mode processing. For bimodal-laser processing, a second laser beam was superimposed, oscillating sinusoidally perpendicular to the scan direction at a frequency of 250 Hz and an offset amplitude of 160 µm while maintaining constant horizontal velocity (Fig. 3d). This oscillating beam also possessed a single-mode profile (Fig. 3e), which forms a similar melt track with a sinusoidal path that mirrors its scan trajectory (Fig. 3f). On the other hand, bimodal-laser processing (Fig. 3g) leads to a dynamic intensity distribution which alternates over time between a single-mode profile, similar to Fig. 3b, and bimodal profile (Fig. 3h), corresponding to the minimum and maximum beam offsets, respectively. This spatiotemporal modulation forms a unique melt track (Fig. 3i), which is not a simple combination of the individual tracks formed by the singlemode processes. To analyze and characterize these microstructures, the metal tracks were cut, and the crosssection was observed via SEM.

Fig. 4 shows macro- and micro-scale SEM crosssections of melt tracks obtained under different laser beam intensity distributions. The rapid melting and subsequent resolidification of the metal substrate upon laser irradiation led to visible changes in the microstructure offering a clear profile between the processed and unprocessed regions. In the case of steady single-mode laser scanning across a metal surface (Fig. 4a), the resolidified cross-section of the melt pool displays a symmetric and parabolic profile (emphasized with a yellow line) with a maximum depth of ~228 μm. The higher-magnification SEM (Fig. 4b) reveals elongated columnar grains that originated at the solid-liquid interface and extend toward the centerline of the melt pool. In the case of the steady single-mode laser scan, the average grain

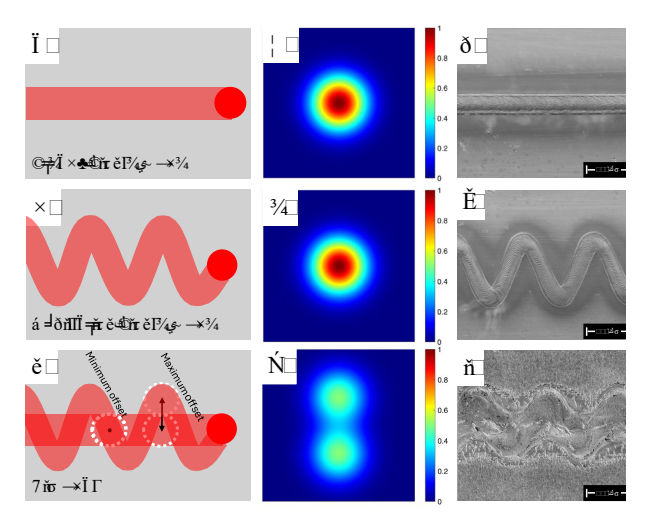


Fig. 3 (a) Schematic of steady single-mode laser processing, (b) beam profile, and (c) top-down view SEM image of resulting melt track. (d) Schematic of oscillating single-mode laser processing, (e) beam profile, and (f) top-down view SEM image of resulting melt track. (g) Schematic of bimodal laser processing, (h) beam profile at maximum offset, and (i) topdown view SEM image of resulting melt track.

length is $\sim 8 \mu m$ and width is $\sim 2 \mu m$, resulting in an aspect ratio of 4 (Fig. 4c). This grain morphology and aspect ratio is indicative of steep thermal gradients on the surface and in the bulk of the metal plate, typical for continuous steadystate heating scenarios.

In contrast, Fig. 4d-i show the bimodal laser scan. The cross-section shown in Fig. 4d is taken at a position of where the two beams are at a minimum offset, corresponding to single-mode. Similarly to Fig. 4a the shape of the melt pool is symmetric and parabolic, but the melt pool depth is smaller than the unmodulated case with a depth of $\sim 200 \, \mu m$. Despite the two laser beams being at a minimum offset, the microstructure in Fig. 3e is different to the microstructure depicted in Fig. 4b. The grains are finer and more equiaxed with an average length of ~4 μm and width of ~2 μm, resulting in an aspect ratio of 2 (Fig. 4f), suggesting a

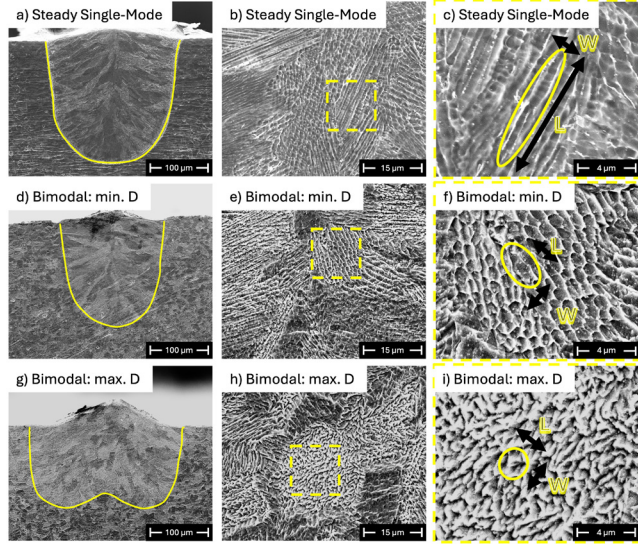


Fig. 4 Progressively higher-magnification cross-sectional SEMs of melt tracks formed by (a-c) steady single-mode, and bimodal laser scan where the offset distance (D) is at a (d-f) minimum or at a (gi) maximum.

smaller thermal gradient due to the oscillatory scan path before and after the overlap.

Fig. 4g shows the cross-section where the two beams were at their maximum offset, corresponding to the bimodal laser scan. Here, the melt pool adopts a dual-lobed shape with two distinct local depth maxima. The two depth maxima are $\sim 150 \, \mu m$ deep. The separation distance between the two depth maxima is 160 µm, which corresponds to the offset amplitude of the oscillating laser. A dual-lobe melt pool shape leads to a broader and shallower melt pool. The microstructure is predominantly equiaxed (Fig. 4h) compared to the unmodulated case (Fig. 4b) with a length and width of $\sim 2 \mu m$, resulting in an aspect ratio of ~ 1 (Fig. 4i). These observations and the aspect ratio suggest that laser beam modulation leads to lower thermal gradients and subsequently more equiaxed grains. A steady single-mode laser scan produces grains with an aspect ratio of ~8, whereas the bimodal laser scan reduces the aspect ratio to ~2 or ~ 1 , promoting a more equiaxed distribution.

To further probe and understand the effects of how bimodal beam modulation influences melt pool dynamics and resulting microstructure, transient three-dimensional finite element method, thermal simulations were conducted using COMSOL Multiphysics® software. Fig. 5 presents a simulated cross-section showing the temperature distribution of the steady single-mode (Fig. 5a), and bimodal laser scan (Fig. 5b), along corresponding directional temperature profiles in x, y, and z (Fig. 5c-e). The simulated melt pool cross-sections and profiles were extracted at a moment of full beam overlap, corresponding to the point of maximum intensity. In the unmodulated case (Fig. 5a), a deep ($\sim 240 \ \mu m$) melt pool is formed. In contrast, even when the two beams are fully overlapped the modulated configuration produces a shallower (~ 205 µm) melt pool (Fig. 5b) despite the same total input energy. The simulated melt pool geometries also show agreement with experimentally observed cross-sections (Fig. 4), supporting the validity of the thermal model.

To assess directional gradients, temperature distributions along the x-, y-, and z-direction (Fig. 5 c-e) from the melt pool center were extracted. Along the scanning direction (xaxis, Fig. 5c), both cases exhibit a peak temperature at the same x-value corresponding to the center of the beam paths. However, the modulated case displays a lower maximum temperature, and respectively reduced gradient. This reduction is attributed to the y-axis modulation of the beam profile, which broadens the spatial energy deposition and reduces the heat flux. Perpendicular to scan direction (y-axis, Fig. 5d), both temperature curves at the surface exhibit parabolic shapes with the steady single-mode being centered and the bimodal laser scan being slightly offset due to the previous oscillation cycle, disrupting directional temperature gradients. The steady single-mode reaches a peak temperature of ~2800 K, while the modulated case peaks at ~2500 K. The temperature gradient is again steeper for the steady single-mode case (~2700 K/mm) than the bimodal laser scan (~1800 K/mm), consistent with a more localized heat input. Into the metal plate (z-axis, Fig. 5e), the temperature continuously decreases with depth for both configurations. The steady single-mode starts at a maximum temperature of ~2800 K at the surface, compared to ~2500 K for the modulated case, which results in a shallower

temperature gradient. Although the absolute temperature difference is moderate, prior studies have shown that even relatively small reductions in thermal gradient can shift

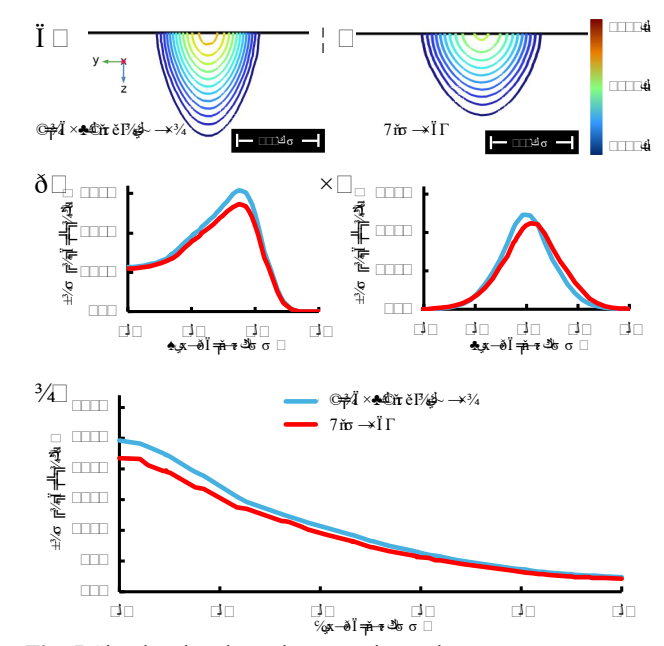


Fig. 5 Simulated melt pool geometries and temperature contours for (a) steady single-mode and (b) bimodal laser scan and temperature profiles along (c) the x-direction (scanning direction), (d) y-direction and (e) the z-direction for steady single-mode (blue) and bimodal (red).

solidification behavior from columnar to equiaxed [27,28].

Across all directions, the bimodal beam configuration leads to reduced thermal gradients compared to the steady single-mode. These thermal conditions are known to promote equiaxed grain formation by suppressing directional solidification along the heat flow. In contrast to simple beam defocusing, which lowers intensity uniformly in a single-mode, bimodal configuration in the form of two superimposed beams introduces spatially and temporally varying heat input and induces complex heat flows, actively changing the thermal profiles and disrupting unidirectional solidification paths. These variations suppress directional solidification and facilitate the formation of equiaxed grain structures. As a result, bimodal beam shaping dynamically tailors melt pool dimensions (SEMs in Fig. 4) and cooling rates (COMSOL in Fig. 5), enabling refined and more equiaxed microstructures.

4. Conclusion

This study investigates the effects of bimodal-laser beam shaping on microstructures resulting from the melting and resolidification of stainless steel. The superimposing of an oscillation beam results in a broader and more shallow melt pool compared to a steady single-mode scan. Cross-sectional SEMs indicate dynamic beam shaping leads to modified melt pool geometries and the formation of more equiaxed grain growth. COMSOL simulations show that the temperature gradients are lower in the bimodal laser scan, and the oscillations are and disrupting directional solidification paths, even when the total energy input remains constant. These findings highlight the advantages of a bimodal-laser setup, where beam oscillation not only modifies the thermal profile but also promotes favorable

conditions for equiaxed grain formation. When considered alongside previous work[24] demonstrating the benefits of oscillating beams for surface quality enhancement, the current results suggest that bimodal-laser beam modulation offers a promising and versatile strategy for simultaneously optimizing both surface features and grain structure. This makes it a compelling approach for future applications in additive manufacturing and other laser-based metal processing techniques.

Acknowledgments

This work was jointly funded by Princeton University, the Office of Naval Research, and Kitware Inc., under Sponsor Award Number K004522-00-S01 (PRIME ONR # N68335-24-C-0039). Characterizations were conducted using the facilities of the Princeton Imaging and Analysis Center (IAC) which is partially supported by the Princeton Center for Complex Materials, a National Science Foundation (NSF)-MRSEC program (DMR-2011750).

References

- [1] R. McCann, M.A. Obeidi, C. Hughes, É. McCarthy, D.S. Egan, and R.K. Vijayaraghavan: Addit. Manuf., 45, (2021) 102058.
- [2] L. Li, M. Hong, M. Schmidt, M. Zhong, A. Malshe, and B. Huis in't Veld: CIRP Ann., 60, (2011) 735.
- [3] M. Rupp, S. Hayashi, C. Dashe, S. Gupta, R. Moini, and C.B. Arnold: Appl. Phys. A, 129, (2023) 64.
- [4] S. Hayashi, X. Du, M. Rupp, K.A. Filsinger, M. Terakawa, and C.B. Arnold: Opt. Laser Technol., 174, (2024) 110686.
- [5] S. Hayashi, A. Sanchirico, A. Das, and C.B. Arnold: Appl. Phys. Lett., 126, (2025) 041601.
- [6] S. Hayashi, M. Rupp, J.X. Liu, J.W. Stiles, A. Das, A. Sanchirico, and C.B. Arnold: Adv. Sci., (2024) 2412588.
- [7] A. Das and C.-F. Ding: Small Methods, 8, (2023) 2301429.
- [8] A. Piqué, R.C.Y. Auyeung, H. Kim, N.A. Charipar, and S.A. Mathews: J. Phys. D: Appl. Phys., 49, (2016) 223001.
- [9] M.S. Brown and C.B. Arnold: "Laser Precision Microfabrication," ed. by K. Sugioka, M. Meunier, and A. Piqué, (Springer, Berlin, 2010) p.91.

- [10] A. Das, D. Ghosh, S.-F. Lau, P. Srivastava, A. Ghosh, and C.-F. Ding: Adv. Eng. Inform., 62, (2024) 102932.
- [11] A. Das, S.S. Sarkar, A. Ghosh, S. Chattopadhyaya, N. Gubeljak, and A. Kumar: Int. J. Adv. Manuf. Technol., 123, (2022) 3337.
- [12] C. Teng, D. Pal, H. Gong, K. Zeng, K. Briggs, and N. Patil: Addit. Manuf., 14, (2017) 137.
- [13] M. Seiler, A. Patschger, L. Tianis, C. Rochholz, and J. Bliedtner: J. Laser Appl., 29, (2017) 022413.
- [14] P. Oyar: Photomed. Laser Surg., 36, (2017) 72.
- [15] P. Berger, H. Hügel, and T. Graf: Phys. Procedia, 12, (2011) 241.
- [16] C. Forster, M. Döring, C. Spurk, M. Hummel, A. Olowinsky, and F. Beckmann: Procedia CIRP, 124, (2024) 464.
- [17] T. Niendorf, S. Leuders, A. Riemer, H.A. Richard, T. Tröster, and D. Schwarze: Metall. Mater. Trans. B, 44, (2013) 794.
- [18] T.T. Roehling, R. Shi, S.A. Khairallah, J.D. Roehling, and G.M. Guss, J.T. McKeown: Mater. Des., 195, (2020) 109071.
- [19] L.H. Shah, F. Khodabakhshi, and A. Gerlich: J. Manuf. Process., 37, (2019) 212.
- [20] M. Rupp, K. Schwarzkopf, M. Döring, S. Hayashi, M. Schmidt, and C.B. Arnold: J. Manuf. Process., 131, (2024) 1624.
- [21] W. Zhang, W. Hou, L. Deike, and C.B. Arnold: Acta Mater., 201, (2020) 14.
- [22] W. Zhang, K. Wong, M. Morales, C. Molpeceres, and C.B. Arnold: Int. J. Extrem. Manuf., 2, (2020) 035101.
- [23] H. Jung, N. Mangelinck-Noël, H. Nguyen-Thi, and B. Billia: J. Alloys Compd., 484, (2009) 739.
- [24] M. Rupp, K. Schwarzkopf, M. Döring, S. Hayashi, M. Schmidt, and C.B. Arnold: J. Manuf. Process., 131, (2024) 1624.
- [25] C.S. Kim: U.S. Dept. Energy Report 4152287 (1975).
- [26] K.C. Mills: "Recommended Values of Thermophysical Properties for Selected Commercial Alloys," (Woodhead Publishing, Cambridge, 2002).
- [27] D.M. Stefanescu and R. Ruxanda: "Fundamentals of Solidification," Metallography and Microstructures, ASM International, (2018) p.71.
- [28] V.P. Narayana Samy, M. Schäfle, F. Brasche, U. Krupp, and C. Haase: Addit. Manuf., 73, (2023) 103702.

(Received: September 6, 2025, Accepted: November 12, 2025)